Diffusion-Weighted Imaging of Skull Lesions

Daniel T. Ginat[1] Rajiv Mangla[2] Gabrielle Yeaney[3] Sven Ekholm[2]

[1] Department of Radiology, University of Chicago Medical Center, Chicago, Illinois, United States
[2] Department of Imaging Sciences, University of Rochester Medical Center, Rochester, New York, United States
[3] Department of Pathology, University of Rochester Medical Center, Rochester, New York, United States

Address for correspondence Daniel T. Ginat, MD, MS, Department of Radiology, University of Chicago Medical Center, 5841 South Maryland Avenue Chicago, IL 60637, United States (e-mail: ginatd01@gmail.com).

J Neurol Surg B 2014;75:204–213.

Abstract

Diffusion-weighted imaging can increase the conspicuity of skull lesions and be applied toward noninvasive differentiation of malignant from benign lesions. Malignant skull lesions generally display lower diffusivity than benign lesions, although there are exceptions, and clinical parameters and conventional imaging modalities should also be considered in the evaluation of skull lesions. Nevertheless, in some instances diffusion-weighted imaging (DWI) can be used for problem solving when conventional imaging features are indeterminate, such as with skull base involvement by nasopharyngeal carcinoma versus osteomyelitis. In addition, DWI may be useful for monitoring treatment effects. The use of readout segmented technique, parallel imaging, multishot acquisition, turbo spin-echo DWI, diffusion tensor imaging, and higher field strengths can improve image quality. The feasibility of implementing DWI for characterizing skull lesions, the DWI findings of benign and malignant skull lesions, and technical considerations are discussed in this article.

Keywords
- skull
- lesions
- apparent diffusion coefficient
- diffusion-weighted imaging
- MRI

Introduction

Diffusion-weighted imaging (DWI) exploits the phenomenon of Brownian motion and can provide information about the functional environment of water in tissues.[1] In particular, DWI can be used to detect shifts of water from extracellular to intracellular spaces, decreased membrane permeability, increased cellular density, and disruption of cellular membrane depolarization, which are findings commonly associated with malignancies.[1] Consequently, DWI has important applications in tumor imaging including tumor detection and characterization as well as assessment of response to therapy.[1]

Because diffusion-weighted images are inherently T2 weighted, tissue T2 properties can affect the appearance of diffusion-weighted images independent of tissue diffusivity, potentially resulting in T2 shine-through and T2 blackout effects [J].[2] These untoward effects can be mitigated by generating apparent diffusion coefficient (ADC) maps, which can be calculated during postprocessing with the use of at least two different b values (degree of diffusion weighting), typically 0 second mm^2 and 1,000 second mm^2. The ADC value is the slope of the line on the plot of the logarithm of relative signal intensity versus b value.

The diffusivity of a lesion can be ascertained by drawing a region of interest in the ADC map and is expressed in units of mm^2/s. Selection of regions of interest (ROIs) is somewhat an art, and there is a paucity of literature dedicated to comparing various measurement techniques for optimizing measurements. It is helpful to reference other sequences for proper positioning of ROIs to avoid including areas of necrosis, calcifications, or hemorrhage that can produce spurious results. We also recommend excluding the edges of the lesions, which may be prone to susceptibility artifacts. In practice, selection of the ROIs may parallel that of the ROIs used in the specific article being referenced. The ADC values of a lesion can be expressed as mean or

received
March 10, 2012
accepted after revision
November 3, 2012
published online
March 12, 2014

DOI http://dx.doi.org/10.1055/s-0034-1371362.
ISSN 2193-6331.

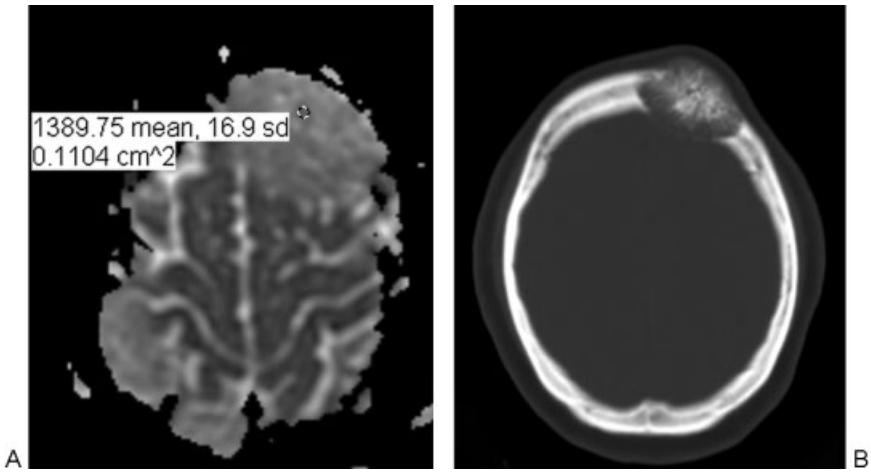

Fig. 1 Intraosseous hemangioma. (A) Apparent diffusion coefficient map with a sample region of interest demonstrates high diffusivity within the left frontal bone lesion. (B) The lesion appears as an expansile mixed lucent and sclerotic intradiploic lesion with a spoke-wheel pattern on the axial computed tomography.

minimum measurements or can be reported as ratios with respect to normal-appearing white matter or soft tissue. Ultimately, it must be cautioned that absolute and cut-off ADC values reported in the literature cannot be easily extrapolated for clinical practice. Indeed, it has been reported that the absolute ADC values for brain parenchyma vary up to 9% for the same vendor and 7% between different vendors.[3]

In general, conventional imaging plays a key role in the assessment of skull lesions. Nevertheless, DWI has been found to improve the conspicuity of metastases when compared with T1-weighted sequences.[4,5] DWI has also proven useful for identifying recurrent tumors and differentiating these from posttreatment changes.[4] Furthermore, significantly higher ADC values have been reported in benign skull base tumors than in malignant lesions.[6,7] However, there are exceptions, most notably low-grade chondrosarcomas, Langerhans cell histiocytosis, and certain metastases.[7] The DWI features of a variety of benign and malignant skull base and calvarial lesions, as well as the technical challenges and future directions with regard to DWI of the skull are discussed in the subsequent sections.

Benign Lesions

Hemangiomas

Intraosseous hemangiomas are benign vascular tumors that comprise 9 to 13% of all calvarial lesions.[8,9] Intraosseous hemangiomas sometimes lack the classic conventional imaging features. In such situations, DWI can be helpful in characterizing these as benign because hemangiomas tend to have high lesion-to-white matter ADC ratios, typically on the order of 1.5 to 1.7 (►**Fig. 1**).[7]

Intradiploic Dermoid and Epidermoid Cysts

Dermoid cysts most commonly occur in the midline, measure < 2 cm, and present in children < 5 years of age.[8] These lesions are often cystic but can also contain fat and calcifications. Epidermoids are benign ectodermal inclusion cysts that comprise 7% of calvarial lesions.[8] Analogous to their

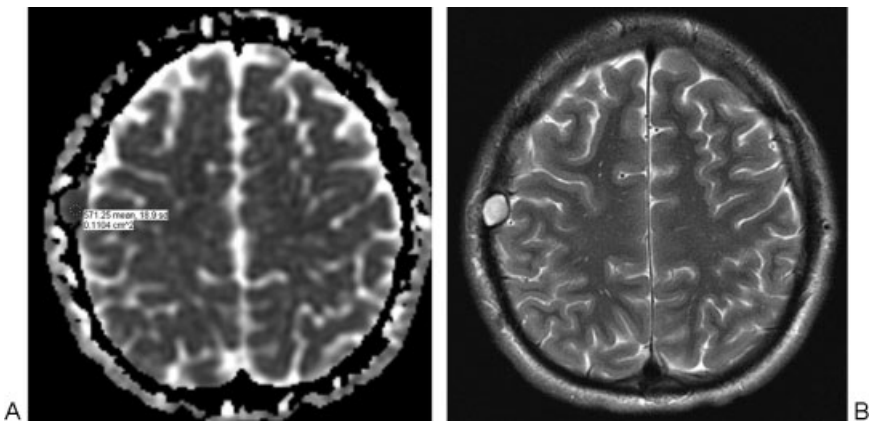

Fig. 2 Intradiploic epidermoid cyst. (A) Apparent diffusion coefficient map with a sample region of interest shows that the right parietal bone lesion has restricted diffusion. (B) The lesion also displays high signal on the T2-weighted MRI.

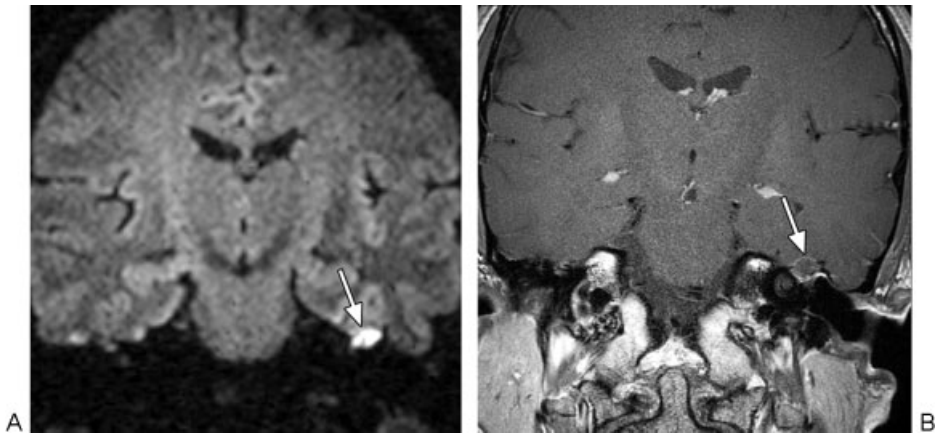

Fig. 3 Recurrent cholesteatoma. (A) Coronal turbo spin-echo diffusion-weighted image shows a hyperintense focus within the right mastoid bowl (arrow). (B) Coronal postcontrast T1-weighted magnetic resonance imaging shows that the lesion does not enhance (arrow).

intracranial counterparts, intradiploic epidermoid cysts can demonstrate high signal on DWI, which may result from T2 shine-through that results in intermediate ADC values in some cases and actual diffusion restriction with low ADC values in other cases (►**Fig. 2**).[10]

Recurrent Cholesteatoma

The 5-year recurrence rate of middle ear cholesteatomas has been reported to be 16.7% in patients treated with canal wall up mastoidectomy.[11] Non–echo-planar imaging (EPI) DWI can potentially serve as an alternative to second-look surgery for the detection of recurrent cholesteatoma. Indeed, non-EPI DWI confers a positive predictive value for cholesteatoma of 93 to 100%.[12,13] On DWI, cholesteatomas appear as hyperintense foci (►**Fig. 3**). However, it is important to interpret the diffusion-weighted images in conjunction with the conventional sequences to avoid false-positive findings that can result from the presence of fat grafts or hemorrhage.

Langerhans Cell Histiocytosis

Langerhans cell histiocytosis can manifest as focal bone lesions that most commonly affect the calvaria in pediatric patients.[14] These lesions tend to have low ADC values relative to white matter (►**Fig. 4**).[7] Consequently, the DWI appearance of Langerhans cell histiocytosis can mimic malignancy and can be ascribed to high cellular density.[7]

Fibrous Dysplasia

Fibrous dysplasia comprises 20% of calvarial lesions, can be monostotic or less commonly polyostotic, and may be associated with McCune-Albright syndrome.[8,14] Fibrous dysplasia with poor contrast enhancement and T2 prolongation tends to display high ADC values, on the order of 2.0×10^{-3} mm^2/s (►**Fig. 5**).[7,15] Fibrous dysplasia comprises 20% of calvarial lesions, can be monostotic or less commonly polyostotic, and may be associated with McCune-Albright syndrome.[5,7]

Intraosseous Meningioma

Primary intraosseous meningiomas comprise $< 2\%$ of meningiomas overall.[16] These lesions mainly involve the calvarium and the spheno-orbital region (►**Fig. 6**). There is a paucity of literature regarding the DWI characteristics of intraosseous meningiomas. However, intracranial meningiomas display highly variable ADC values, whereby DWI has not been found to provide additional value in differentiating the

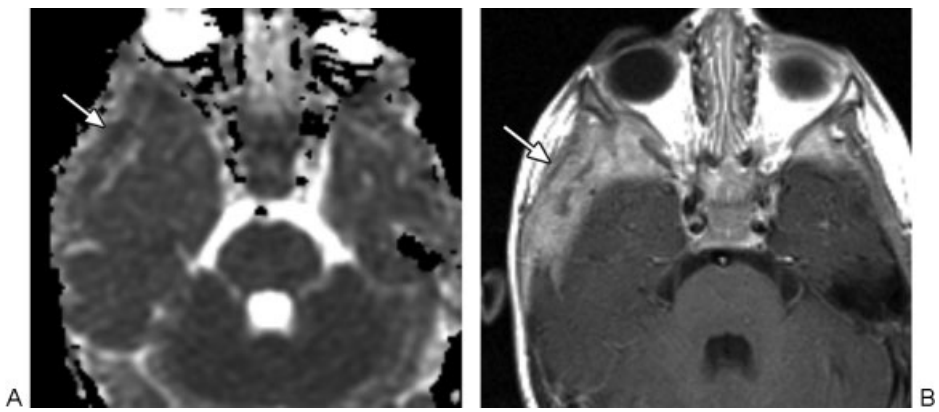

Fig. 4 Langerhans cell histiocytosis. (A) Apparent diffusion coefficient map with a sample region of interest shows restricted diffusion within the lesion (arrow). (B) On T1-weighted postcontrast MRI, the lesion (arrow) appears ill defined and enhances heterogeneously.

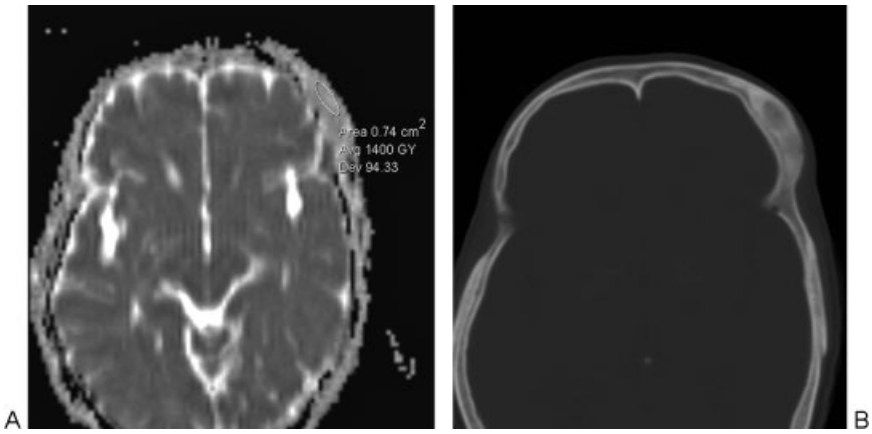

Fig. 5 Fibrous dysplasia. (A) Apparent diffusion coefficient map with a sample region of interest demonstrates high diffusivity throughout the left frontal bone lesion. (B) The corresponding axial computed tomography image shows that the lesion has ground-glass attenuation.

histopathologic subtypes or predicting proliferation indexes.[17,18]

Skull Base Osteomyelitis

Skull base osteomyelitis is an unusual infection that can result from the spread of necrotizing otitis externa, particularly in diabetic patients.[19] On MRI, skull base osteomyelitis often displays decreased T1 signal and enhancement in the affected bone marrow and soft tissues inferior to the skull base, and infiltration and obliteration of the parapharyngeal and retrocondylar fat.[19] A mean ADC 1.26×10^{-3} mm^2/s has been reported in cases of skull base osteomyelitis (►**Fig. 7**), which is higher than most malignant lesions.[19] Thus DWI can enable differentiation of skull base osteomyelitis from malignant neoplasms when conventional imaging and clinical parameters are otherwise equivocal.

Malignant Tumors

Nasopharyngeal Carcinoma

Skull base involvement with nasopharyngeal carcinoma is common, occurring in $>$ 30% of cases.[20] Nasopharyngeal carcinomas display low diffusivity (►**Fig. 8**), with a mean ADC value and ratio normalized to the pons of 0.74×10^{-3} mm^2/s and 0.5, respectively.[19] Thus the diffusivity of nasopharyngeal carcinoma is significantly higher than for skull base osteomyelitis, as stated previously.[19]

Chondrosarcoma

Chondrosarcomas comprise 6% of skull base tumors and tend to display high signal on T2-weighted magnetic resonance imaging (MRI).[21] Low-grade chondrosarcomas tend to have markedly elevated ADC (►**Fig. 9**). An overall ADC value of 2.3×10^{-3} mm^2/s has been reported for chondrosarcomas in the extremities, which is higher than for most benign tumors.[15] Similarly, low-grade chondrosarcoma of the skull base displays high diffusivity reported to be $1.8 \times 10^{-3} mm^2/s$ (►**Fig. 9**).[22] This phenomenon can be explained by the presence of abundant hyaline cartilage with myxoid ground substance and relatively sparse cellularity.[7,23]

Chordoma

Skull base chordomas are uncommon malignancies that most commonly arise in the midline of the clivus and include the conventional, chondroid, and dedifferentiated varieties.[23] Although a midline location favors chordoma over

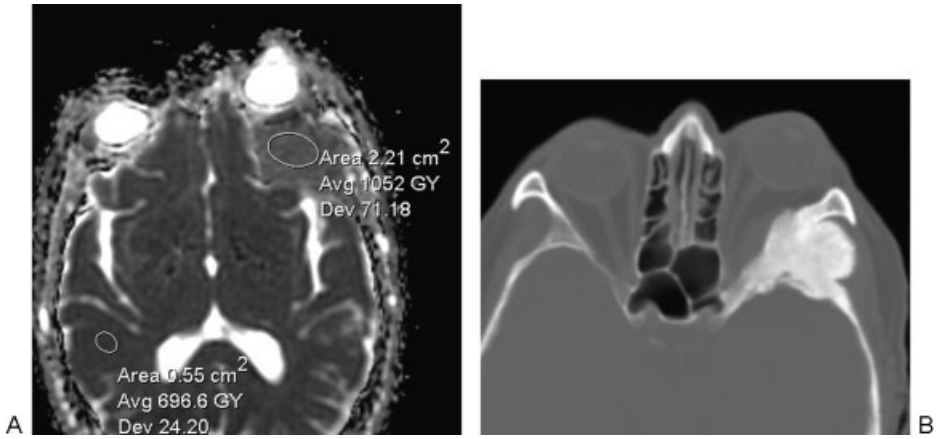

Fig. 6 Intraosseous meningioma. (A) Apparent diffusion coefficient map with a sample region of interest shows elevated diffusivity within the left sphenoid triangle mass. (B) The corresponding axial computed tomography image shows a hyperostotic lesion.

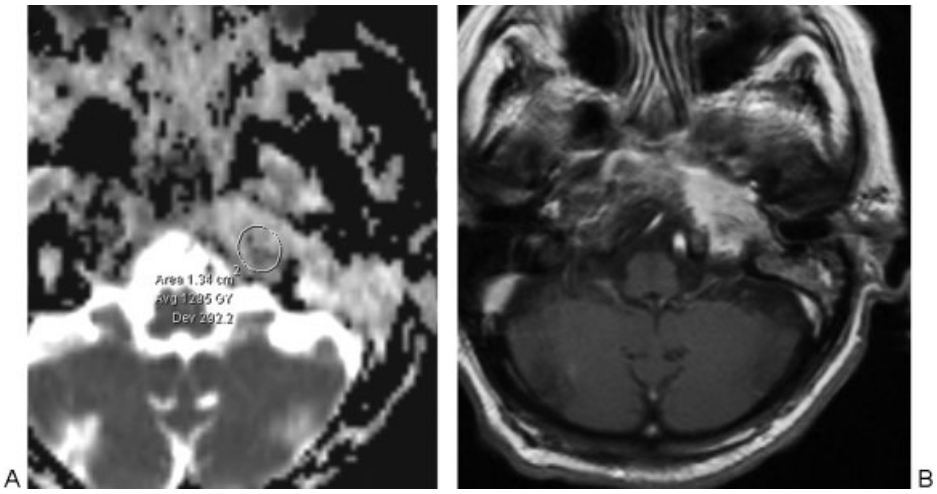

Fig. 7 Skull base osteomyelitis. (A) Apparent diffusion coefficient map with a sample region of interest shows elevated diffusivity within the affected left petrous apex. (B) The corresponding postcontrast T1-weighted image shows ill-defined enhancement.

chondrosarcoma, conventional imaging features cannot always reliably differentiate chordoma from chondrosarcoma. ADC values in conventional chordomas can be elevated (1.5×10^{-3} mm^2/s) but usually to a lesser degree than with low-grade chondrosarcomas (►**Fig. 10**).[7,22] However, poorly differentiated chordomas tend to display restricted diffusion, on the order of 0.9×10^{-3} mm^2/s.[22]

Ewing Sarcoma

Primary cranial Ewing sarcomas are rare malignant neoplasms that tend to affect the pediatric population and comprise 1 to 6% of all Ewing sarcomas.[24,25] Ewing sarcomas contain a densely packed sheet of cells with corresponding restricted diffusion (►**Fig. 11**). However, areas of hemorrhage and necrosis within these tumors may have relatively high ADC values.

Rhabdomyosarcoma

In the pediatric population, rhabdomyosarcoma represents the most common soft tissue sarcoma, comprising up to 5% of childhood malignancies.[26] Rhabdomyosarcoma has a predilection for the craniofacial region. Although no evidence-based data are currently available specifically concerning DWI for rhabdomyosarcomas involving the skull, restricted diffusion can be appreciated in these lesions (►**Fig. 12**). Furthermore, a series that included four cases of rhabdomyosarcomas in the orbit showed that these lesions have distinctly different diffusion characteristics compared with capillary hemangiomas, which can otherwise demonstrate overlapping appearances on conventional MRI sequences.[27]

Multiple Myeloma

Overall, multiple myeloma is the most common primary malignant bone neoplasm in adults and represents proliferation of atypical plasma cells that characteristically produce "punched-out" lytic lesions in the focal form of the disease.[8,28] These lesions tend to display restricted diffusion (►**Fig. 13**).[29] Whole-body DWI is a promising tool for evaluating treatment response in multiple myeloma, in which good

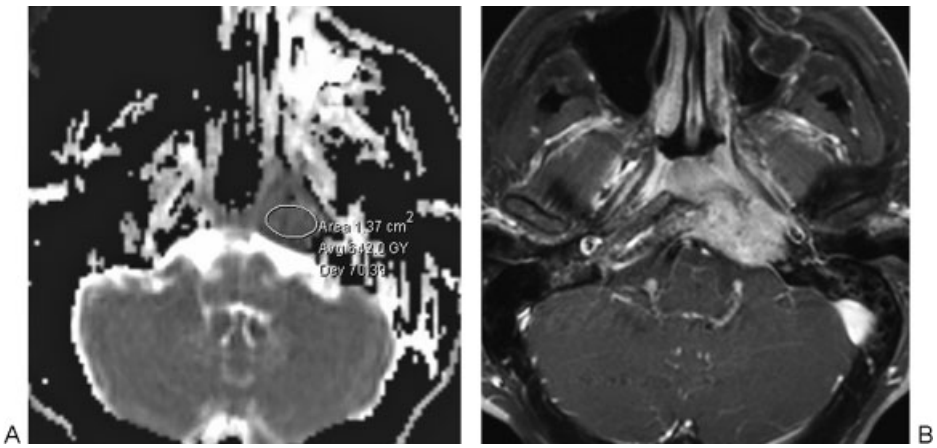

Fig. 8 Nasopharyngeal carcinoma. (A) Apparent diffusion coefficient map with a sample region of interest shows diminished diffusivity within the left central skull base lesion. (B) The corresponding postcontrast T1-weighted magnetic resonance imaging shows enhancement within the lesion that extends from the nasopharynx into the left base clivus.

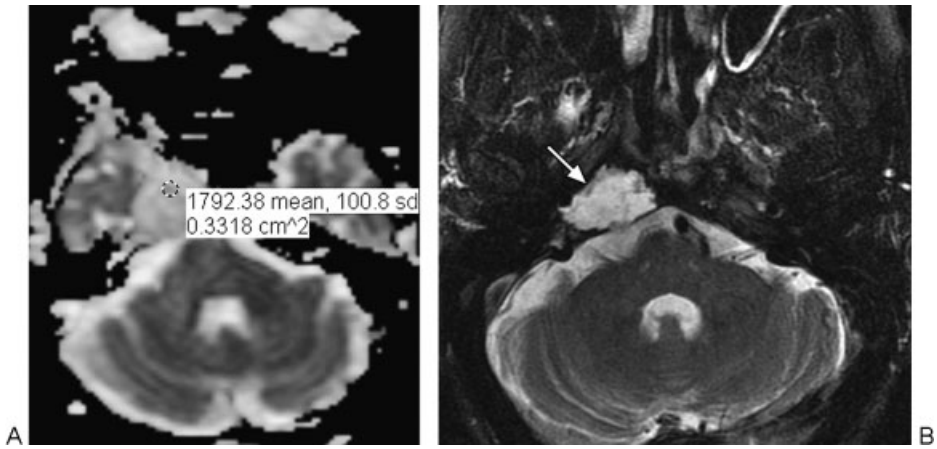

Fig. 9 Low-grade chondrosarcoma. (A) Apparent diffusion coefficient map with a sample region of interest shows high diffusivity throughout the tumor. (B) T2-weighted magnetic resonance imaging shows homogeneous high signal in the mass (arrow).

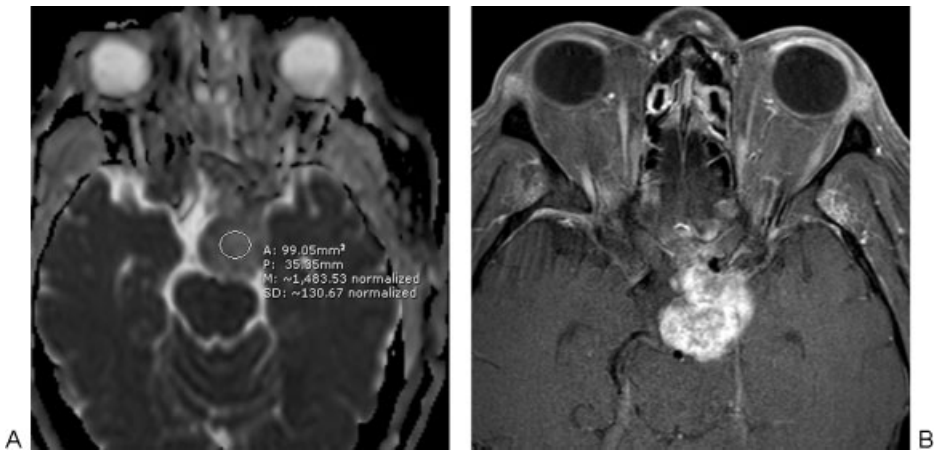

Fig. 10 Conventional chordoma. (A) Apparent diffusion coefficient map with a sample region of interest shows relatively elevated diffusivity in the exophytic clival mass. (B) The corresponding T1-weighted image shows avid enhancement within the mass.

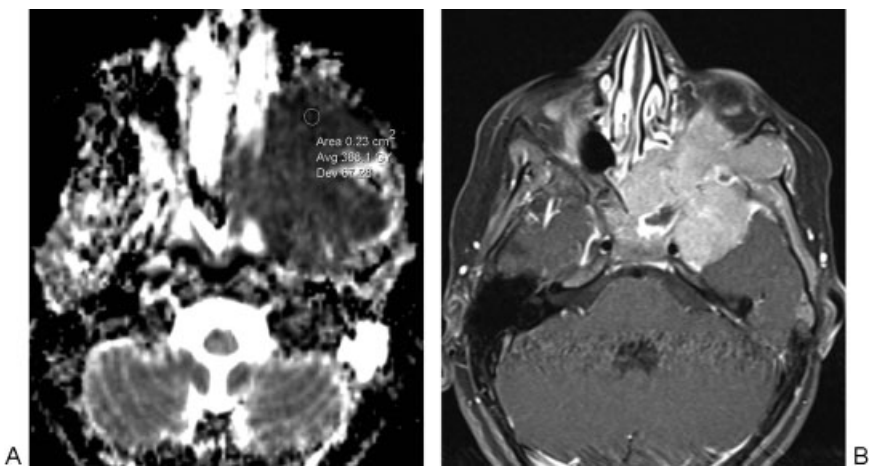

Fig. 11 Ewing sarcoma. (A) Apparent diffusion coefficient map with a sample region of interest depicts restricted diffusion throughout much of the mass. (B) The postcontrast T1-weighted image shows an avidly enhancing irregular mass centered in the greater wing of the left sphenoid bone.

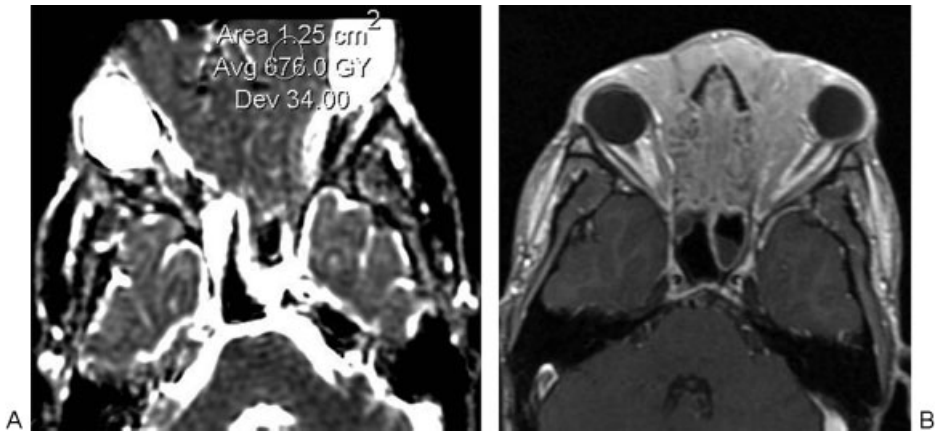

Fig. 12 Rhabdomyosarcoma. (A) Apparent diffusion coefficient map with sample region of interest shows a large mass that involves the anterior cranial fossa. (B) Axial postcontrast T1-weighted image shows a diffusely enhancing mass.

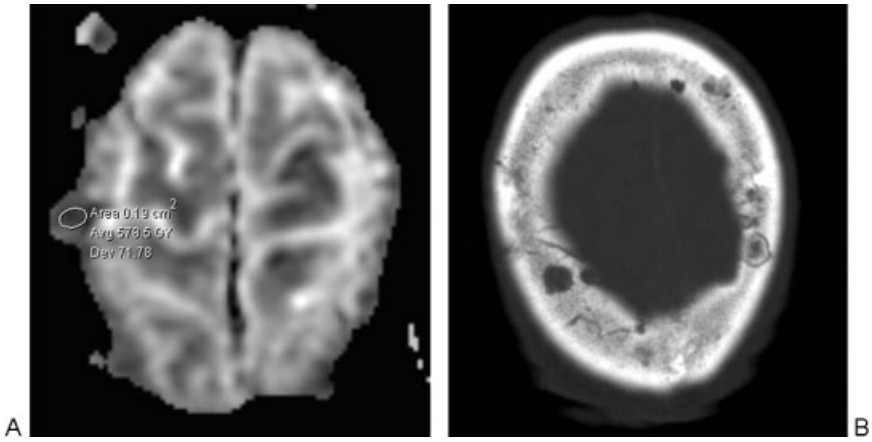

Fig. 13 Multiple myeloma. (A) Apparent diffusion coefficient map with a sample region of interest shows several calvarial lesions with relatively low diffusivity. (B) Axial computed tomography image shows several punched-out lytic lesions in the skull.

response correlates with increased ADC values compared with baseline.[29]

Lymphoma

Primary non-Hodgkin lymphoma of the cranium is a rare condition.[19,30] Lymphomas in the skull base region have ADC values in the range of 0.51 to 0.59 $\times$ 10^{-3} mm^2/s (►**Fig. 14**), which are significantly lower than for nasopharyngeal carcinomas and skull base osteomyelitis.[19,30]

Metastases

Skull metastases most commonly arise from breast, prostate, and lung primaries in adults, and neuroblastoma in children.[8] DWI improves the conspicuity of metastatic lesions over conventional MRI (►**Fig. 15**).[3,4] Skull metastases are a histologically diverse group of lesions that results in a wide range of ADC values with a mean value reported to be $0.99 \pm 0.34 \times 10^{-3}$ mm^2/s.[19] Consequently, there is overlap in the ADC values of metastases with other malignant lesions, such as lymphoma and nasopharyngeal carcinoma, as well as benign entities, such as osteomyelitis.[19] However, it has been observed that metastatic sarcomas generally display lower ADC values than carcinomas.[31]

Technical Considerations

A particular challenge toward implementing conventional EPI DWI in the skull is the presence of susceptibility changes at tissue interfaces, such as at the skull base and paranasal sinus regions. This leads to image distortion and artifacts, which limits the application of standard single-shot EPI DWI for the detection of lesions at tissue interfaces, especially when using ultrahigh field strength. Susceptibility effects that result in geometric distortion also tend to be more severe with increasing b-values. Geometric distortion can be reduced by implementing readout segmented EPI sequences compared with single-shot EPI.[32] In readout segmented sequences, segments of k-space are acquired along the readout direction, which decreases readout time.

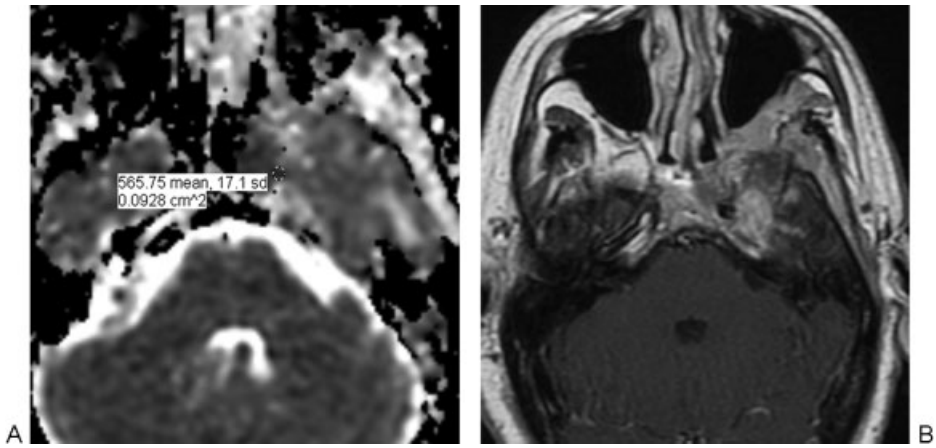

Fig. 14 Lymphoma. (A) Apparent diffusion coefficient map with a sample region of interest shows restricted diffusion in the lesion adjacent to the left cavernous sinus. (B) The lesion enhances homogenously on the postcontrast T1-weighted image.

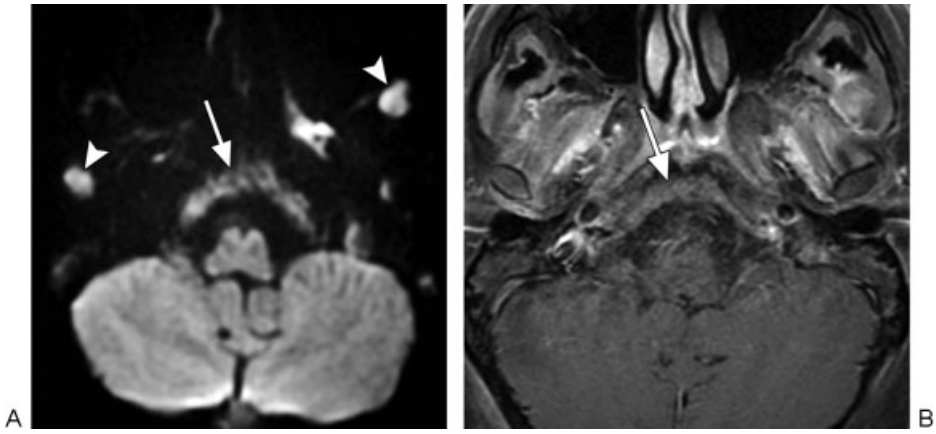

Fig. 15 Metastases. (A) Diffusion-weighted imaging shows diffuse involvement of the clivus by metastatic disease (arrow). There are additional metastatic lesions within the bilateral masticator spaces (arrowheads). (B) The clivus lesion (arrow) is less conspicuous on the corresponding postcontrast T1-weighted image.

Multishot acquisition and parallel imaging are two techniques that have been applied to DWI to diminish distortions and increase spatial resolution for skull base imaging. Multishot sequences enable a single image to be reconstructed from k-space data acquired separately after two or more radiofrequency excitations (shots). This results in considerably less degradation from off-resonance effects than with single-shot techniques. For instance, compared with single-shot EPI, multi-shot EPI offers greater accuracy for the diagnosis of acquired middle ear cholesteatomas.[33] Parallel imaging, such as sensitivity encoding, decreases the total readout duration by sampling fewer lines of k-space, with the missing data inferred from the coil sensitivity profiles. The decreased readout time reduces artifacts related to magnetic field inhomogeneities in long echo train sequences.[34]

Implementation of EPI diffusion-weighted sequences in the skull is limited by susceptibility artifact and relatively low resolution. Rather, turbo spin-echo DWI has proven to be more reliable than EPI DWI for the diagnosis of skull base lesions such as cholesteatomas.[35,36] Indeed, using turbo spin-echo DWI, cholesteatomas as small as 2 mm can be detected.[36]

The increased signal-to-noise ratios achieved with higher field strength magnets can potentially improve the quality of ADC maps for head and neck lesions compared with conventional field strengths, without additional degradation of the images by susceptibility artifact. The use of 3.0 T appears to improve DWI assessment of skull base tumors adjacent to the paranasal sinuses and petrous air cells over 1.5-T MRI. Shimming on a slice-by-slice basis can significantly improve field homogeneity at high field strengths.[37] In addition, the impact of the susceptibility artifacts can also be mitigated through the use of thinner sections.

Diffusion tensor imaging may also offer superior image quality over conventional DWI of skull base lesions. The improved signal-to-noise achieved with diffusion tensor imaging is attributable to acquisition of data in many directions; however, the additional information pertaining to directionality is not necessarily relevant to skull lesions.

In the future, DWI may be used to monitor the response to nonsurgical therapies and distinguish between posttreatment changes and recurrent skull lesions. For example, in head and neck squamous cell carcinoma, ADC maps have 87 to

95% accuracy in discriminating between tumoral and non-tumoral tissues following chemotherapy.[38,39] Posttherapeutic changes tend to display higher ADC values than the original or recurrent tumors.

Conclusion

DWI of skull tumors is feasible and in some cases useful for predicting benign versus malignant etiology. Indeed, benign skull lesions generally display higher ADC values than their malignant counterparts. However, the high ADC values observed in chordomas and low-grade chondrosarcomas, the low ADC values in eosinophilic granuloma, and the variable ADC values in metastatic disease are potential pitfalls for DWI. The use of techniques, such as parallel imaging, multishot, turbo spin-echo sequence, diffusion tensor imaging, and higher field strengths can improve on standard single-shot EPI DWI for evaluating skull lesions. Ultimately, DWI of skull lesions must not be interpreted in isolation. Rather, the findings on this technique should be integrated into a holistic assessment in conjunction with conventional imaging modalities and clinical parameters.

References

1 Malayeri AA, El Khouli RH, Zaheer A, et al. Principles and applications of diffusion-weighted imaging in cancer detection, staging, and treatment follow-up. Radiographics 2011;31(6):1773–1791
2 Hiwatashi A, Kinoshita T, Moritani T, et al. Hypointensity on diffusion-weighted MRI of the brain related to T2 shortening and susceptibility effects. AJR Am J Roentgenol 2003;181(6):1705–1709
3 Sasaki M, Yamada K, Watanabe Y, et al; Acute Stroke Imaging Standardization Group-Japan (ASIST-Japan) Investigators. Variability in absolute apparent diffusion coefficient values across different platforms may be substantial: a multivendor, multi-institutional comparison study. Radiology 2008;249(2):624–630
4 Moon WJ, Lee MH, Chung EC. Diffusion-weighted imaging with sensitivity encoding (SENSE) for detecting cranial bone marrow metastases: comparison with T1-weighted images. Korean J Radiol 2007;8(3):185–191
5 Nemeth AJ, Henson JW, Mullins ME, Gonzalez RG, Schaefer PW. Improved detection of skull metastasis with diffusion-weighted MR imaging. AJNR Am J Neuroradiol 2007;28(6):1088–1092
6 Abdel Razek A, Mossad A, Ghonim M. Role of diffusion-weighted MR imaging in assessing malignant versus benign skull-base lesions. Radiol Med (Torino) 2011;116(1):125–132
7 Ginat DT, Mangla R, Yeaney G, Johnson M, Ekholm S. Diffusion-weighted imaging for differentiating benign from malignant skull lesions and correlation with cell density. AJR Am J Roentgenol 2012;198(6):W597-601
8 Lloret I, Server A, Taksdal I. Calvarial lesions: a radiological approach to diagnosis. Acta Radiol 2009;50(5):531–542
9 Khanam H, Lipper MH, Wolff CL, Lopes MB. Calvarial hemangiomas: report of two cases and review of the literature. Surg Neurol 2001;55(1):63–67; discussion 67
10 Chen S, Ikawa F, Kurisu K, Arita K, Takaba J, Kanou Y. Quantitative MR evaluation of intracranial epidermoid tumors by fast fluid-attenuated inversion recovery imaging and echo-planar diffusion-weighted imaging. AJNR Am J Neuroradiol 2001;22(6):1089–1096
11 Mishiro Y, Sakagami M, Kitahara T, Kondoh K, Okumura S. The investigation of the recurrence rate of cholesteatoma using Kaplan-Meier survival analysis. Otol Neurotol 2008;29(6):803–806
12 De Foer B, Vercruysse JP, Bernaerts A, et al. Detection of postoperative residual cholesteatoma with non-echo-planar diffusion-weighted magnetic resonance imaging. Otol Neurotol 2008; 29(4):513–517
13 Dremmen MH, Hofman PA, Hof JR, Stokroos RJ, Postma AA. The diagnostic accuracy of non-echo-planar diffusion-weighted imaging in the detection of residual and/or recurrent cholesteatoma of the temporal bone. AJNR Am J Neuroradiol 2012;33(3):439–444
14 Hayden Gephart MG, Colglazier E, Paulk KL, Vogel H, Guzman R, Edwards MS. Primary pediatric skull tumors. Pediatr Neurosurg 2011;47(3):198–203
15 Hayashida Y, Hirai T, Yakushiji T, et al. Evaluation of diffusion-weighted imaging for the differential diagnosis of poorly contrast-enhanced and T2-prolonged bone masses: Initial experience. J Magn Reson Imaging 2006;23(3):377–382
16 Arana E, Diaz C, Latorre FF, et al. Primary intraosseous meningiomas. Acta Radiol 1996;37(6):937–942
17 Ginat DT, Mangla R, Yeaney G, Wang HZ. Correlation of diffusion and perfusion MRI with Ki-67 in high-grade meningiomas. AJR Am J Roentgenol 2010;195(6):1391–1395
18 Sanverdi SE, Ozgen B, Oguz KK, et al. Is diffusion-weighted imaging useful in grading and differentiating histopathological subtypes of meningiomas? Eur J Radiol 2012;81(9):2389–2395
19 Ozgen B, Oguz KK, Cila A. Diffusion MR imaging features of skull base osteomyelitis compared with skull base malignancy. AJNR Am J Neuroradiol 2011;32(1):179–184
20 Sham JS, Cheung YK, Choy D, Chan FL, Leong L. Nasopharyngeal carcinoma: CT evaluation of patterns of tumor spread. AJNR Am J Neuroradiol 1991;12(2):265–270
21 Meyers SP, Hirsch WL Jr, Curtin HD, Barnes L, Sekhar LN, Sen C. Chondrosarcomas of the skull base: MR imaging features. Radiology 1992;184(1):103–108
22 Yeom KW, Lober RM, Mobley BC, et al. Diffusion-weighted MRI: distinction of skull base chordoma from chondrosarcoma. AJNR Am J Neuroradiol 2013;34(5):1056–1061, S1
23 Bourgouin PM, Tampieri D, Robitaille Y, et al. Low-grade myxoid chondrosarcoma of the base of the skull: CT, MR, and histopathology. J Comput Assist Tomogr 1992;16(2):268–273
24 Li WY, Brock P, Saunders DE. Imaging characteristics of primary cranial Ewing sarcoma. Pediatr Radiol 2005;35(6):612–618
25 Moschovi M, Alexiou GA, Tourkantoni N, et al. Cranial Ewing's sarcoma in children. Neurol Sci 2011;32(4):691–694
26 Freling NJ, Merks JH, Saeed P, et al. Imaging findings in craniofacial childhood rhabdomyosarcoma. Pediatr Radiol 2010;40(11): 1723–1738; quiz 1855
27 Lope LA, Hutcheson KA, Khademian ZP. Magnetic resonance imaging in the analysis of pediatric orbital tumors: utility of diffusion-weighted imaging. J AAPOS 2010;14(3):257–262
28 Hanrahan CJ, Christensen CR, Crim JR. Current concepts in the evaluation of multiple myeloma with MR imaging and FDG PET/CT. Radiographics 2010;30(1):127–142
29 Baur-Melnyk A, Buhmann S, Becker C, et al. Whole-body MRI versus whole-body MDCT for staging of multiple myeloma. AJR Am J Roentgenol 2008;190(4):1097–1104
30 Maeda M, Maier SE, Sakuma H, Ishida M, Takeda K. Apparent diffusion coefficient in malignant lymphoma and carcinoma involving cavernous sinus evaluated by line scan diffusion-weighted imaging. J Magn Reson Imaging 2006;24(3):543–548
31 Srinivasan A, Dvorak R, Perni K, Rohrer S, Mukherji SK. Differentiation of benign and malignant pathology in the head and neck using 3T apparent diffusion coefficient values: early experience. AJNR Am J Neuroradiol 2008;29(1):40–44
32 Iima M, Yamamoto A, Brion V, et al. Reduced-distortion diffusion MRI of the craniovertebral junction. AJNR Am J Neuroradiol 2012; 33(7):1321–1325
33 Yamashita K, Yoshiura T, Hiwatashi A, et al. Detection of middle ear cholesteatoma by diffusion-weighted MR imaging: multishot

echo-planar imaging compared with single-shot echo-planar imaging. AJNR Am J Neuroradiol 2011;32(10):1915–1918
34 Glockner JF, Hu HH, Stanley DW, Angelos L, King K. Parallel MR imaging: a user's guide. Radiographics 2005;25(5):1279–1297
35 De Foer B, Vercruysse JP, Pilet B, et al. Single-shot, turbo spin-echo, diffusion-weighted imaging versus spin-echo-planar, diffusion-weighted imaging in the detection of acquired middle ear cholesteatoma. AJNR Am J Neuroradiol 2006;27(7):1480–1482
36 De Foer B, Vercruysse JP, Bernaerts A, et al. The value of single-shot turbo spin-echo diffusion-weighted MR imaging in the detection of middle ear cholesteatoma. Neuroradiology 2007;49(10):841–848
37 Curtis AT, Gilbert KM, Klassen LM, Gati JS, Menon RS. Slice-by-slice B1+ shimming at 7 T. Magn Reson Med 2012;68(4):1109–1116
38 Vandecaveye V, De Keyzer F, Nuyts S, et al. Detection of head and neck squamous cell carcinoma with diffusion weighted MRI after (chemo)radiotherapy: correlation between radiologic and histopathologic findings. Int J Radiat Oncol Biol Phys 2007;67(4):960–971
39 Abdel Razek AA, Kandeel AY, Soliman N, et al. Role of diffusion-weighted echo-planar MR imaging in differentiation of residual or recurrent head and neck tumors and posttreatment changes. AJNR Am J Neuroradiol 2007;28(6):1146–1152